

This is a repository copy of *Triaxial deformation of neutron-rich Zr nuclei explored by high-resolution in-beam  $\gamma$ -ray spectroscopy*.

White Rose Research Online URL for this paper:

<https://eprints.whiterose.ac.uk/218313/>

Version: Published Version

---

**Article:**

Moon, B., Korten, W., Wimmer, K. et al. (26 more authors) (2024) Triaxial deformation of neutron-rich Zr nuclei explored by high-resolution in-beam  $\gamma$ -ray spectroscopy. *Physics Letters B*. 139047. ISSN 0370-2693

<https://doi.org/10.1016/j.physletb.2024.139047>

---

**Reuse**

This article is distributed under the terms of the Creative Commons Attribution (CC BY) licence. This licence allows you to distribute, remix, tweak, and build upon the work, even commercially, as long as you credit the authors for the original work. More information and the full terms of the licence here:

<https://creativecommons.org/licenses/>

**Takedown**

If you consider content in White Rose Research Online to be in breach of UK law, please notify us by emailing [eprints@whiterose.ac.uk](mailto:eprints@whiterose.ac.uk) including the URL of the record and the reason for the withdrawal request.



## Letter



# Triaxial deformation of neutron-rich Zr nuclei explored by high-resolution in-beam $\gamma$ -ray spectroscopy

B. Moon<sup>a,b,\*,</sup>, W. Korten<sup>c</sup>, K. Wimmer<sup>d,e,b,f</sup>, P. Doornenbal<sup>b</sup>, T.R. Rodríguez<sup>g</sup>, N. Aoi<sup>h</sup>, H. Baba<sup>b</sup>, F. Browne<sup>b</sup>, C. Campbell<sup>i</sup>, S. Chen<sup>j,k</sup>, H. Crawford<sup>i</sup>, H. de Witte<sup>l</sup>, C. Fransen<sup>m</sup>, H. Hess<sup>m</sup>, E. Ideguchi<sup>h</sup>, S. Iwazaki<sup>h</sup>, J. Kim<sup>n,o</sup>, N. Kitamura<sup>p</sup>, A. Kohda<sup>h</sup>, T. Koiwai<sup>f</sup>, B. Mauss<sup>b</sup>, R. Mizuno<sup>f</sup>, M. Niikura<sup>f</sup>, T. Parry<sup>q</sup>, P. Reiter<sup>m</sup>, H. Sakurai<sup>b,f</sup>, D. Suzuki<sup>b</sup>, R. Taniuchi<sup>j</sup>, S. Thiel<sup>m</sup>, Y. Yamamoto<sup>h</sup>

<sup>a</sup> Center for Exotic Nuclear Studies, Institute for Basic Science, Daejeon 34126, Republic of Korea

<sup>b</sup> RIKEN Nishina Center, 2-1 Hirosawa, Wako, Saitama 351-0198, Japan

<sup>c</sup> IRFU, CEA, Université Paris-Saclay, F-91191 Gif-sur-Yvette, France

<sup>d</sup> GSI Helmholtzzentrum für Schwerionenforschung GmbH, Planckstr. 1, 64291 Darmstadt, Germany

<sup>e</sup> Instituto de Estructura de la Materia, CSIC, E-28006 Madrid, Spain

<sup>f</sup> Department of Physics, University of Tokyo, 7-3-1 Hongo, Bunkyo, Tokyo 113-0033, Japan

<sup>g</sup> Departamento de Estructura de la Materia, Física Térmica y Electrónica and IPARCOS, Universidad Complutense de Madrid, 28040 Madrid, Spain

<sup>h</sup> Research Center for Nuclear Physics (RCNP), Osaka University, Mihogaoka, Ibaraki, Osaka 567-0047, Japan

<sup>i</sup> Nuclear Science Division, Lawrence Berkeley National Laboratory, Berkeley, CA 94720, USA

<sup>j</sup> School of Physics, Engineering and Technology, University of York, Heslington, York YO10 5DD, United Kingdom

<sup>k</sup> Department of Physics, The University of Hong Kong, Pokfulam 999077, Hong Kong

<sup>l</sup> Institute for Nuclear and Radiation Physics, KU Leuven, Leuven B-3001, Belgium

<sup>m</sup> Institut für Kernphysik, Universität zu Köln, D-50937 Cologne, Germany

<sup>n</sup> Department of Physics, Korea University, Seoul 02841, Republic of Korea

<sup>o</sup> Center for Extreme Nuclear Matters, Korea University, Seoul 02841, Republic of Korea

<sup>p</sup> Center for Nuclear Study, University of Tokyo, RIKEN campus, Wako, Saitama 351-0198, Japan

<sup>q</sup> Department of Physics, University of Surrey, Guildford GU2 7XH, United Kingdom

## ARTICLE INFO

Editor: B. Blank

## Keywords:

Triaxial deformation  
Harmonic-oscillator shell closure  
Lifetime measurement  
In-beam  $\gamma$ -ray spectroscopy

## ABSTRACT

Lifetimes of excited states in the very exotic nuclides  $^{108}\text{Zr}_{68}$  and  $^{110}\text{Zr}_{70}$  were measured for the first time applying high-resolution in-beam  $\gamma$ -ray spectroscopy at relativistic energies. The experiment was carried out at the Radioactive Isotope Beam Factory in RIKEN, using nucleon removal reactions of radioactive Nb ions to produce  $^{108}\text{Zr}$  and  $^{110}\text{Zr}$ . Emitted  $\gamma$  rays from the excited states were measured by the High-resolution Cluster Array at RIBF (HiCARI) and lifetimes were extracted from the observed line shapes caused by relativistic Doppler-shift effects. In addition to the new lifetime information, the precision of the  $E(2_1^+)$  and  $R_{4/2} = E(4_1^+)/E(2_1^+)$  values of  $^{110}\text{Zr}$  could be significantly improved. The low-lying  $2_2^+$  states in both nuclei are also newly observed, which are indicative of the triaxiality. The various physical quantities were compared with theoretical models to investigate the collectivity in Zr isotopes towards  $N = 70$ . Together the experimental and theoretical results point at a reduction of the axial deformation while triaxial collectivity increases.

The nuclear shell structure is one of the cornerstones for a comprehensive understanding of the atomic nucleus, since the first correct description of closed shells at the so-called magic numbers was achieved by including a strong spin-orbit term by M. Goeppert-Mayer and O. Haxel [1–3]. However, strong evidence has been collected over

the last decades, that these magic numbers are not universal, but subject to changes when going away from the valley of stability. In the absence of a large energy gap at the shell closures, the maximum binding energy of the nucleus departs from spherical symmetry and nuclei is deformed in their ground states. Shell evolution has been subject of

\* Corresponding author at: Center for Exotic Nuclear Studies, Institute for Basic Science, Daejeon 34126, Republic of Korea.  
E-mail addresses: [mb0316@ibs.re.kr](mailto:mb0316@ibs.re.kr) (B. Moon), [w.korten@cea.fr](mailto:w.korten@cea.fr) (W. Korten), [k.wimmer@gsi.de](mailto:k.wimmer@gsi.de) (K. Wimmer).

intense experimental investigations and is now firmly established for light and medium heavy nuclei, e.g., at neutron numbers  $N = 8, 20$ , and  $28$ . In all cases, the onset of deformation is observed when removing protons from the doubly closed-shell nuclei,  $^{16}\text{O}$ ,  $^{40}\text{Ca}$  and  $^{48}\text{Ca}$ , respectively [4]. Evidence for the erosion of the shell closure in heavier nuclei at  $N = 50, 82$ , and  $126$  which are induced by the strong spin-orbit interaction, is still rather scarce since the isotopes of interest below and/or beyond the doubly-magic core are experimentally extremely difficult to reach.

The zirconium (Zr) isotopes with the harmonic-oscillator proton shell closure ( $Z = 40$ ) represent one of the key cases for the understanding of this shell evolution and the onset of deformation in atomic nuclei. The isotopes  $^{90}\text{Zr}$  and  $^{96}\text{Zr}$ , at neutron numbers  $N = 50$  and  $56$ , respectively, exhibit properties of doubly-magic nuclei with high-lying first excited  $2^+$  states and low  $B(E2)$  transition rates [5]. However, a sudden onset of deformation appears at  $N = 60$  in  $^{100}\text{Zr}$ , which has a low-lying  $2^+$  state and a very large  $B(E2)$  value [5]. This abrupt shape transition is due to the strong proton-neutron ( $\pi$ - $\nu$ ) interaction between the overlapping  $\pi g_{9/2}$ - $\nu g_{7/2}$  spin-orbit partner orbitals [6]. For isotopes up to  $N = 58$  ( $^{98}\text{Zr}$ ), the spherical configuration is dominant in the ground state, while the deformed configuration lies at higher excitation energy, but becomes the ground state in  $^{100}\text{Zr}$ . This crossing of two configurations with different deformation (here spherical and strongly deformed) is evidence of the type II shell evolution [7–9]. The heavier Zr isotopes beyond  $N = 60$  are all strongly deformed in their ground states, but an onset of triaxial deformation is expected by several theoretical models [10,11]. Evidence for triaxiality has been found experimentally in the Mo isotopes [12], but for the Zr isotopes further information on the excitation energies of ground-band and higher-lying states, and the transition strengths between these states is needed.

The heaviest Zr isotopes for which spectroscopic information is available are  $^{108}\text{Zr}$  [13] and  $^{110}\text{Zr}$  [11]. Contrary to the expectation that the combination of harmonic-oscillator quantum numbers  $Z = 40$  and  $N = 70$  might favor a spherical shape [14,15], their low-lying  $2^+$  states indicated substantial deformation also for these isotopes. Nevertheless, important questions about their structure remain open, such as the possibility of shape coexistence or triaxial deformation when approaching  $N = 70$  as predicted by different theoretical models: Monte-Carlo shell-model calculations predict a prolate ground state and a triaxial shape for the excited-state band structure [16], while different beyond-mean field models using the Gogny interaction predict a triaxial ground state and a prolate excited  $0_2^+$  state [11]. Consequently, more spectroscopic information on the Zr isotopes toward  $N = 70$  is essential to understand the structure of these exotic isotopes.

In this letter, the first lifetime measurement of excited states in  $^{108}\text{Zr}$  and  $^{110}\text{Zr}$  through the line-shape method [17] is reported to address these questions. Moreover, the spectroscopic information on  $^{110}\text{Zr}$  could be significantly improved. Finally, the experimental results are compared to different state-of-the-art nuclear model calculations.

The experiment was carried out at the Radioactive Isotope Beam Factory (RIBF). A cocktail beam was produced by in-flight fission of a  $^{238}\text{U}$  primary beam bombarding a 4-mm thick  $^9\text{Be}$  target at an energy of 345 A MeV. The fission fragments were selected and identified in the BigRIPS spectrometer through the  $B\rho$ - $\Delta E$ -Time-of-Flight method [18,19]. In a secondary reaction,  $^{108}\text{Zr}$  was produced on a 6-mm thick  $^9\text{Be}$  target at about 225 A MeV by the one-proton and one-neutron removal from  $^{110}\text{Nb}$ , while  $^{110}\text{Zr}$  nuclides were produced by the one-proton removal reaction from  $^{111}\text{Nb}$ . These Nb isotopes represented a fraction of 1.6% and 0.8% of the secondary beam, respectively.

The projectile-like reaction products were transmitted through the ZeroDegree Spectrometer (ZDS) and identified by the same method as in BigRIPS. Emitted  $\gamma$  rays were measured by the High-resolution Cluster Array at RIBF (HiCARI) [20]. In the present experiment, the setup was optimized for best efficiency and sensitivity to long lifetimes, and therefore the 6-mm thick  $^9\text{Be}$  target was placed 10 cm upstream of the nominal target position. Six Miniball triple-cluster detectors [21] were

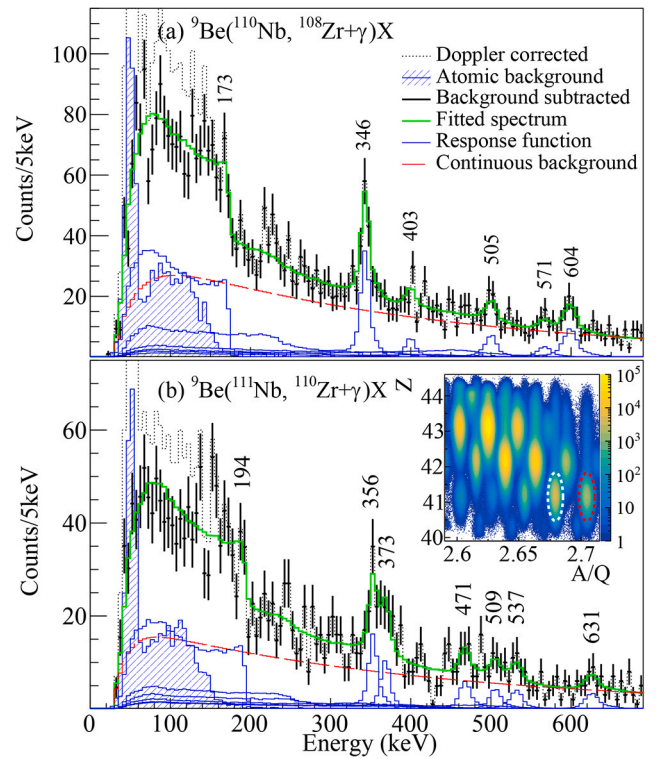


**Fig. 1.** Doppler-corrected energy spectra of (a)  $^{108}\text{Zr}$  and (b)  $^{110}\text{Zr}$  measured by the six Miniball detectors at forward angles. The black dotted and black solid lines are energy spectra before and after the atomic background (blue-dashed filled) subtractions, respectively. The data are superimposed by the results of a fit (green lines) of individual response functions obtained from the simulation (blue solid lines) and a continuous background (red dashed lines). The inset represents the particle identifications in the BigRIPS spectrometer. White- and red-dashed circles are  $^{110}\text{Nb}$  and  $^{111}\text{Nb}$ , respectively.

mounted under the most forward angles covering  $15^\circ$  to  $35^\circ$  with respect to the beam direction. Four segmented clover detectors [22] were installed to cover the angle range of  $38^\circ$ – $65^\circ$  together with two modules of GRETTINA-type tracking detectors [23]. The energy calibrations were performed using  $^{152}\text{Eu}$  and  $^{133}\text{Ba}$   $\gamma$ -ray sources. The intrinsic energy resolution is, however, small compared to the large Doppler effects at relativistic energies. The Doppler correction was applied assuming that the interaction point with the highest energy deposit was the first interaction of a photon with the detector material. For the tracking detectors the interaction points were derived from the signal decomposition as described in Ref. [24]. For the segmented detectors, the segment center, determined from the average of first interactions in the simulation, was employed. The precise positioning of the detectors with respect to the laboratory system was achieved by photogrammetry measurements. The Miniball detectors show better sensitivity to longer lifetimes, while the clover and tracking detectors have less sensitivity to long lifetimes due to the larger angles with respect to the target and significantly lower statistics. Consequently, only the Miniball detectors were used for the following analysis. Their total  $\gamma$ -ray peak detection efficiency at rest amounted to  $\sim 1.5\%$  at 0.3 MeV.

Figs. 1(a) and (b) represent the Doppler-corrected energy spectra of  $^{108}\text{Zr}$  and  $^{110}\text{Zr}$ , respectively. Since the lifetimes of the  $2^+$  states are expected to be longer than the traversal time through the target of  $\sim 35$  ps, the Doppler correction employed the velocity after the target with a mean value of  $v/c \sim 0.525$ . The  $2^+ \rightarrow 0_1^+$  transitions in both nuclei are located below 200 keV. Therefore, the prompt atomic background dominating in the low-energy region had to be subtracted. This was obtained from a measurement of the  $\gamma$ -ray spectrum in coincidence with the unreacted beams, similar to the previous work [11]. In the resulting background-subtracted spectra the line shapes of the  $2^+ \rightarrow 0_1^+$

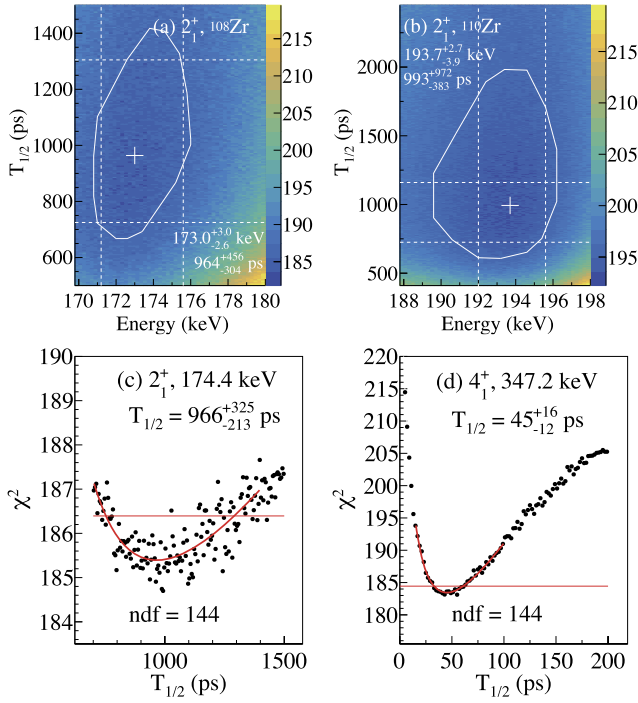


**Fig. 2.** The  $\chi^2$  maps of the  $2_1^+ \rightarrow 0_1^+$  transitions of (a)  $^{108}\text{Zr}$  and (b)  $^{110}\text{Zr}$  as a function of transition energies and half-lives are shown, respectively. The minimum  $\chi^2$  values are marked with white crosses, and the corresponding energy and half-life values are given with their statistical errors only. The solid white contour indicates the area where energy and half-life simultaneously take on values within the  $1\sigma$  range of the optimum values. The straight dashed lines mark the  $1\sigma$  ranges of energies and half-lives extracted independently. The one-dimensional  $\chi^2$  plots of the (c) 174.4-keV and (d) 347.2-keV transitions in  $^{108}\text{Zr}$  obtained by fixing their transition energies known from decay spectroscopy. Red curves and horizontal lines are fit results and  $\chi^2_{\min} + 1.0$  limits for  $\pm 1\sigma$  errors, respectively.

transitions exhibit long tails, which are indicative of the long lifetime. This effect can be employed to determine the lifetime of the emitting state [17].

Since the Doppler-corrected energy spectrum was significantly affected by the lifetime effect, the standard fitting method using a Gaussian function plus continuous background could not be employed. Instead, the response function of the Ge detectors obtained from the simulation for all transitions, including the lifetime effect was used. For this purpose, a customized Geant4 [25] simulation package, based on the GRETINA simulation software [26], was employed to obtain the HiCARI response function to  $\gamma$  rays of different energies and half-lives emitted in-flight [27]. The Doppler correction for the simulated data was performed in the same way as described above for the experimental data. The resulting spectra, including a background function composed of two exponential functions, were fitted to the experimental spectra as shown in Fig. 1. These response functions were simulated in steps of 0.2-keV for all transition energies, while for the half-lives 5-ps steps were applied for the  $2_1^+ \rightarrow 0_1^+$  transitions, and 2-ps steps were used for all other transitions. For each simulation, a  $\chi^2$  value was obtained by comparing the simulated response function with the experimental spectrum using the  $\chi^2$  fit method. In this way, the two-dimensional  $\chi^2$  maps could be obtained as shown for the  $2_1^+ \rightarrow 0_1^+$  transitions in  $^{108}\text{Zr}$  and  $^{110}\text{Zr}$  in Figs. 2(a) and (b).

The mean values and  $1\sigma$  errors for the transition energy and half-life were obtained from the 2-dimensional (2D)  $\chi^2$  maps. The white crosses in Figs. 2(a) and (b) indicate the best-fitting  $E - T_{1/2}$  combination obtained from the minimum  $\chi^2_{\min}$  of a smoothed  $\chi^2$  surface. The white solid lines in Figs. 2(a) and (b) show the  $\chi^2_{\min} + 2.4$  contours,

**Table 1**

Summary of transition energies, half-lives (not including feeding effects), assignments, and transition rates in  $^{108}\text{Zr}$  and  $^{110}\text{Zr}$  obtained from the present work. The theoretical  $B(E2)$  values from the HFB-SCCM calculations [30] are given for comparison. Uncertainties include both statistical and systematic errors.

$E_\gamma$ (keV)	$T_{1/2}$ (ps)	$J_i^\pi$	$J_f^\pi$	$B(E2; J_i^\pi \rightarrow J_f^\pi)$ (W.u.)	
$^{108}\text{Zr}_{68}$				exp.	SCCM
$173_{-3}^{+3}$	$966_{-235}^{+340a}$	$2_1^+$	$0_1^+$	$103_{-33}^{+33}$	83
$346_{-3}^{+3}$	$45_{-12}^{+16a}$	$4_1^+$	$2_1^+$	$81_{-21}^{+29}$	121
$403_{-8}^{+3}$	$< 128$	$(2_2^+)$	$2_1^+$	$> 6^c$	88
$505_{-8}^{+6}$	$44_{-36}^{+136}$	$(2_2^+)$	$2_1^+$	$13_{-10}^{+61}$	
$571_{-9}^{+8}$	$< 94$	$(2_2^+)$	$0_1^+$	$> 3$	0.85
$604_{-7}^{+5}$	$41_{-18}^{+27a}$	$(3_1^+)$	$2_1^+$	$6_{-2}^{+4c}$	2
$^{110}\text{Zr}_{70}$				exp.	SCCM
$194_{-3}^{+3}$	$993_{-972}^{+977}$	$2_1^+$	$0_1^+$	$61_{-39}^{+51}$	70
$356_{-4}^{+3}$	$32_{-22}^{+44}$	$(4_1^+)$	$2_1^+$	$98_{-52}^{+233}$	106
$373_{-4}^{+3}$	$< 109$	$(2_2^+)$	$2_1^+$	$> 13^c$	105
$471_{-3}^{+3}$	$(25)^b$				
$509_{-7}^{+8}$	$(25)^b$				
$537_{-7}^{+7}$	$51_{-30}^{+115}$			$8_{-6}^{+23}$	
$631_{-10}^{+8}$	$27_{-23}^{+30}$	$(3_1^+)$	$2_1^+$	$1.2_{-0.9}^{+14.0c}$	0.8

<sup>a</sup> These values are obtained by fixing the transition energies from previous decay spectroscopy [29] to reduce the uncertainties.

<sup>b</sup> A typical half-life of 25 ps was employed to obtain the transition energy.

<sup>c</sup> Pure E2 transitions are assumed based on their assignment as transitions from the  $\gamma$  band to the ground-state band and in accordance with the theoretical calculations (see below).

which denote the area where the probability that both energy and half-life simultaneously take on values within one standard deviation and thus include the correlated uncertainties [28]. In addition, the region where the probability that either energy or half-life is in the  $1\sigma$  range is indicated by the dashed lines ( $\chi^2_{\min} + 1$  limits). In general, uncertainties were derived using the former method of the simultaneous joint probabilities, however for 174.4, 347.2, and 603.9-keV transitions in  $^{108}\text{Zr}$  the half-lives were derived with a constraint on the transition energies from decay spectroscopy [29] to validate the analysis. The one-dimensional  $\chi^2$  distributions obtained with these constraints on the energies are shown in Figs. 2(c) and (d). They were fitted by asymmetric Gaussian functions to obtain the best fitting values for half-lives as well as appropriate  $\chi^2_{\min}$  values. The  $1\sigma$  uncertainties were then derived in the standard way using the  $\chi^2_{\min} + 1.0$  limit indicated by the horizontal lines. It is worth noting that all half-lives are consistent with the ones directly obtained from the two-dimensional  $\chi^2$  map (see the case of the 174.4-keV transition in Figs. 2(a) and (c) as an example). For the 403- and 571-keV transitions in  $^{108}\text{Zr}$  and the 373-keV transition in  $^{110}\text{Zr}$  the limited statistics allowed to extract only upper limits for the half-lives. Therefore, the uncertainty on the energy was derived with the  $\chi^2_{\min} + 1$  method.

All measured energies and half-lives are summarized in Table 1. Uncertainties include both statistical and systematic errors, the latter being dominated by the subtraction for the atomic background, which is critical for the  $2_1^+ \rightarrow 0_1^+$  transitions. By changing the normalization factor of the atomic background spectra by  $\pm 10\%$ , the obtained half-lives varied within 100 ps. Therefore, this systematic error was included in the final errors of the half-lives of the  $2_1^+ \rightarrow 0_1^+$  transitions. The energy spectra overlaid with the best-fitting simulation results of the individual transitions are shown in Fig. 1.

In  $^{108}\text{Zr}$ , half-lives of  $966_{-235}^{+340}$  and  $45_{-12}^{+16}$  ps were obtained for the  $173_{-3}^{+3}$ -keV and  $346_{-3}^{+3}$ -keV transitions, respectively. In addition, new transitions at  $403_{-8}^{+3}$ ,  $505_{-8}^{+6}$ , and  $571_{-9}^{+8}$  keV could be observed. In the absence of reliable  $\gamma$ - $\gamma$  coincidence information, these transitions could not be placed in the level scheme with certainty. Nevertheless, the  $403_{-8}^{+3}$  and  $571_{-9}^{+8}$ -keV transitions are tentatively assigned to the decays of the

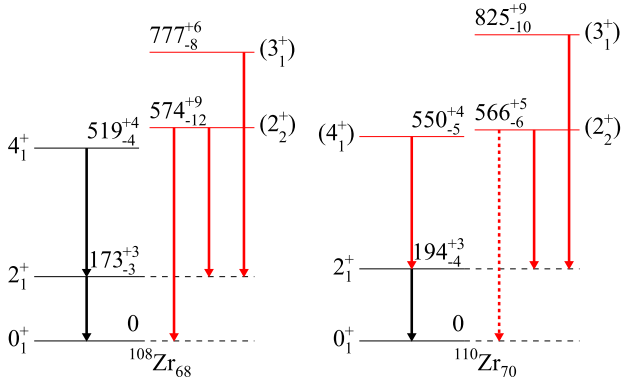


**Fig. 3.** Level schemes of  $^{108}\text{Zr}$  and  $^{110}\text{Zr}$  with excitation energies in keV from the present work. Solid red lines indicate newly observed and tentatively assigned transitions and excited states. The dotted red line marks the unobserved  $(2_2^+) \rightarrow 0_1^+$  transition in  $^{110}\text{Zr}$ .

$2_2^+$  state to the  $2_1^+$  and  $0_1^+$  states, respectively, based on their energy difference of  $168_{-12}^{+9}$  keV which coincides with the excitation energy of the  $2_1^+$  state. In contrast to the previous isomer decay study [29], the  $604_{-7}^{+5}$ -keV transition is now tentatively assigned as the  $(3_1^+) \rightarrow 2_1^+$  decay based on systematics of the relative energy difference in the  $\gamma$  band between the  $3_1^+$  and  $2_2^+$  states (203 keV) in  $^{110}\text{Mo}$  (206 keV) and  $^{112}\text{Ru}$  (224 keV) isotopes [5]. These new assignments are confirmed by the preliminary result of a new isomer decay spectroscopy experiment [31]. The  $505_{-8}^{+6}$ -keV transition is a candidate for the  $6_1^+ \rightarrow 4_1^+$  decay based on its energy, however the measured half-life of  $44_{-36}^{+136}$  ps is not compatible with the value of  $\sim 5$  ps found in lighter and neighboring nuclei such as  $^{98-104}\text{Zr}$  and  $^{104-112}\text{Mo}$  [5,32,33].

In the case of  $^{110}\text{Zr}$ , the simultaneous fitting of transition energy and half-life of the  $2_1^+$  level results in  $194_{-4}^{+3}$  keV and  $993_{-395}^{+977}$  ps. The energy value is slightly larger than the previous result of 185(11) keV [11], which could not take into account the long half-life of this state. A doublet of transitions is observed at  $356_{-4}^{+3}$  and  $373_{-4}^{+4}$  keV, which could not be resolved in the previous work [11]. The  $356_{-4}^{+3}$ -keV transition with a half-life of  $32_{-22}^{+44}$  ps is tentatively assigned to the  $(4_1^+) \rightarrow 2_1^+$  decay. Following the systematics of the Zr isotopes, the  $373_{-4}^{+4}$ -keV transition is a candidate for the  $(2_2^+) \rightarrow 2_1^+$  decay. However, in this case the  $(2_2^+) \rightarrow 0_1^+$  transition, expected at an energy of 566 keV, could not be observed. From the observed intensity limit, we estimate a branching ratio of  $\leq 15\%$  with respect to the  $(2_2^+) \rightarrow 2_1^+$  transition. This estimate leads to a ratio  $B(E2; 2_2^+ \rightarrow 2_1^+)/B(E2; 2_2^+ \rightarrow 0_1^+) \geq 50 \pm 10$ . Such a large ratio was so far observed only in a few Pt isotopes [34–36] and is a strong indication of increased triaxiality in  $^{110}\text{Zr}$ . The assignment of the  $4_1^+$  and  $2_2^+$  states is strongly based on the intensities of the respective transitions. However, in the view of limited statistics and the absence of the  $2_2^+ \rightarrow 0_1^+$  transition the opposite assignment cannot be ruled out. Moreover, the new assignment of the  $2_2^+$  state differs from the previous interpretation [11]. The previously observed 480-keV transition, which was assigned as  $(2_2^+) \rightarrow 0_1^+$ , is now resolved as three different transitions. Among those transitions, a transition at  $537_{-8}^{+7}$ -keV could be analogous to the (unassigned)  $505_{-8}^{+6}$ -keV transition in  $^{108}\text{Zr}$ . The transition at  $631_{-10}^{+8}$ -keV could be analogous to the  $604_{-7}^{+5}$ -keV transition in  $^{108}\text{Zr}$ , leading to a tentative assignment of the  $(3_1^+)$  state at  $825_{-10}^{+9}$  keV. The new level schemes of  $^{108}\text{Zr}$  and  $^{110}\text{Zr}$  proposed from the present work are illustrated in Fig. 3.

In order to discuss the properties of the neutron-rich Zr isotopes, the quantities of  $E(2_1^+)$ ,  $R_{4/2} = E(4_1^+)/E(2_1^+)$ ,  $B(E2; 2_1^+ \rightarrow 0_1^+)$ , and  $R_{2/2} = E(2_2^+)/E(2_1^+)$  are represented in Fig. 4. In the case of  $^{110}\text{Zr}$ , due to the high-resolution  $\gamma$ -ray detection setup the uncertainty for the  $2_1^+$  and  $4_1^+$  excitation energies could be significantly reduced. The  $R_{4/2}$  ratios

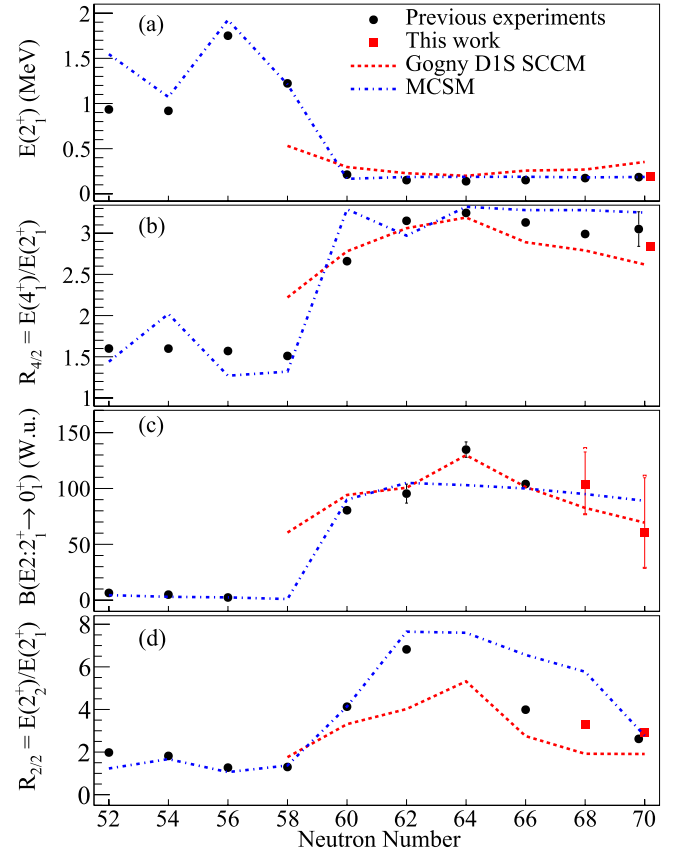


**Fig. 4.** Systematic plots of (a)  $E(2_1^+)$ , (b)  $R_{4/2} = E(4_1^+)/E(2_1^+)$ , (c)  $B(E2; 2_1^+ \rightarrow 0_1^+)$ , and (d)  $R_{2/2} = E(2_2^+)/E(2_1^+)$  values as a function of neutron number. Theoretical results from the SCCM [30] with the Gogny D1S interaction [37,38] and MCSM [16] calculations are shown to compare with the experimental data [11,5,39]. The error bars show the statistical uncertainties, while the caps represent the total errors including the systematic uncertainties, dominated by the atomic background subtraction.

further follow the already observed downward trend from the rigid-rotor limit of  $R_{4/2} = 3.33$  beginning at  $N = 64$ . This fact, together with the slight increase in  $E(2_1^+)$ , suggests a lower degree of (axial) deformation or increased triaxiality towards  $N = 70$ . For the reduced transition probabilities,  $B(E2; 2_1^+ \rightarrow 0_1^+) = 103_{-27}^{+33}$  and  $61_{-32}^{+51}$  W.u. were obtained for  $^{108}\text{Zr}$  and  $^{110}\text{Zr}$ , respectively. These values are of similar magnitude as in the lighter isotopes, but a certain downwards trend towards  $N = 70$  is observed despite the relatively large uncertainties.

The new data also allowed for the identification of candidates of  $2_2^+$  states, which are commonly interpreted as  $\gamma$ -vibrational excitation, i.e., oscillations deviating from axial symmetry. The very low excitation energies of the  $2_2^+$  states in  $^{108}\text{Zr}$  and  $^{110}\text{Zr}$ , coming very close to the  $4_1^+$  states, are thus a strong indication of the importance of non-axial deformation. Interestingly, the transition intensities from the  $2_2^+$  states in  $^{108}\text{Zr}$  and  $^{110}\text{Zr}$  are notably different. The  $2_2^+ \rightarrow 2_1^+$  transition in  $^{110}\text{Zr}$  is very predominant, while in  $^{108}\text{Zr}$  both transitions have comparable intensities. In nuclei with triaxial deformation, the  $2_2^+ \rightarrow 0_1^+$  transition is strongly suppressed compared to the  $2_2^+ \rightarrow 2_1^+$  decay. The transition rate of the  $2_2^+$  state in  $^{110}\text{Zr}$  agrees with this despite the large uncertainties in accordance with an increasing triaxiality.

In order to get further insights into the structure of neutron-rich Zr isotopes, the present data are compared with two state-of-the-art theoretical models. Monte-Carlo shell model (MCSM) calculations were very successful in describing the sudden onset of deformation at  $N = 60$  [16]. These calculations predict strongly axial deformed ground states for  $^{100}\text{Zr}$  onward. While the spectroscopic properties of  $^{108}\text{Zr}$  and

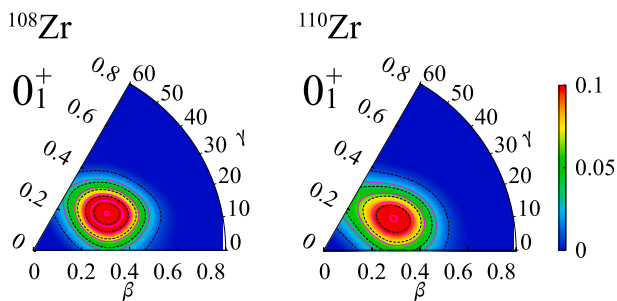


Fig. 5. Potential energy surfaces of the ground states in  $^{108}\text{Zr}$  and  $^{110}\text{Zr}$  from the HFB-SCCM calculations [30].

$^{110}\text{Zr}$  are generally well reproduced, the  $R_{4/2}$  ratio and the location of the  $\gamma$  band are significantly over-predicted, which reflect the axially-deformed ground states. A triaxial excited band is predicted to be built on a low-lying  $0_2^+$  state in  $^{110}\text{Zr}$ , however such a state could not be observed in the present work. A  $\gamma$ -vibrational band is also predicted and can be associated with the observed  $2_2^+$  and  $3_1^+$  states. For  $^{110}\text{Zr}$ , the  $2_2^+$  state energy is well predicted, but the calculations fail to reproduce the smooth evolution of the  $\gamma$ -band head from mid-shell at  $N = 66$ , as shown in Fig. 4(d). The sudden intrusion of a state with a rather well localized minimum at  $\gamma \sim 30^\circ$  in the potential energy surface with  $B(E2)$  values consistent with the rigid-triaxial Davydov and Filippov model [40] as predicted by the MCSM calculations [16], seems thus at variance with the data. It is worth noting that preliminary calculations employing a new Quasiparticle Vaqua Shell Model [41] with a modified Hamiltonian have been developed, which predict an earlier onset of ground states with triaxial shapes already at  $^{108}\text{Zr}$  [42].

The second model is the symmetry-conserving configuration-mixing (SCCM) method [30] using the Gogny D1S interaction [37,38]. In this model, a set of quadrupole-deformed, angular-momentum and particle-number projected Hartree-Fock-Bogolyubov (HFB) states are obtained by minimizing the particle-number projected energy with constraints in the quadrupole degrees of freedom. This method allows for the interpretation of the individual nuclear states in terms of the probability of having certain axial and triaxial shapes in the wave function. The SCCM calculations predict a maximum of collectivity at  $N = 64$ , supported by the minimum in  $E(2_1^+)$  and local maxima for  $B(E2)$  and  $R_{4/2}$ , in good agreement with the data. Specifically, this model reproduces well the decreasing pattern of the  $R_{4/2}$  values beyond  $N = 64$ . The calculations predict a transition from prolate ground-state deformation at  $N = 64$  to almost maximum triaxiality beyond. For the ground-state rotational band, a value of  $\gamma \approx 30^\circ$  for  $^{108}\text{Zr}$  and  $^{110}\text{Zr}$  is predicted, as shown in Fig. 5. It is worth noting that the transition rates in the ground state band agree well with the experimental results (see Table 1). The  $2_2^+$  state is predicted to be also triaxial deformed with a similar  $(\beta_2, \gamma)$  deformation that explains the large  $B(E2; 2_2^+ \rightarrow 2_1^+)$  values and almost negligible decay branches to the ground state ( $B(E2; 2_2^+ \rightarrow 0_1^+) = 0.002 e^2 b^2$ ). Above 1 MeV of excitation energy two bands with axial prolate and oblate deformation are predicted. Their experimental verification will be subject to future experiments.

In summary, in the first high-resolution in-beam  $\gamma$ -ray spectroscopy campaign at RIBF employing the HiCARI array, precise excitation energies and excited state lifetimes of the neutron-rich  $^{108}\text{Zr}$  and  $^{110}\text{Zr}$  isotopes were determined for the first time. Despite low production cross sections, the powerful combination of high intensity beams and high-resolution in-beam  $\gamma$ -ray spectroscopy allowed to start disentangling the complex level scheme of  $^{110}\text{Zr}$  and to measure for the first time lifetimes of excited states. A reduction of  $B(E2)$  values and  $R_{4/2}$  ratios from mid-shell implies a decrease in axial deformation. Low-lying  $2_2^+$  states and their decay branching ratios suggest enhanced triaxial deformation which is even increasing in  $^{110}\text{Zr}$  from  $^{108}\text{Zr}$ . While this exploratory research finds evidence for the importance of triaxial degrees of freedom,

further insight into the shape degrees of freedom will require experiments using  $4\pi$   $\gamma$ -ray tracking spectrometers.

This work was carried out at the RIBF operated by RIKEN Nishina Center and Center for Nuclear Studies in the University of Tokyo. We acknowledge the Miniball Collaboration for the loan of the Miniball detectors and supporting frame. Research Center for Nuclear Physics in Japan, Institute of Modern Physics in China, and Lawrence Berkeley National Laboratory and Argonne National Laboratory in USA are also acknowledged for the loan of the detectors and data acquisition electronics. The HiCARI campaign was supported by the JSPS KAKENHI of Japan under the Grant Nos. Kiban-A JP19H00670 and JP19H01914. B. Moon acknowledges supports from Institute for Basic Science (IBS) (Grant No. IBS-R031-Y1) and National Research Foundation (NRF) (Grant No. 2019R1A6A3A03031564) of the Republic of Korea. K. Wimmer acknowledges funding from the Spanish Ministerio de Ciencia, Innovación y Universidades (Grant No. RYC-2017-22007) and the European Research Council (ERC) under the European Union's Horizon 2020 research and innovation programme (grant agreement No. 101001561). T. R. Rodríguez acknowledges funding from the Spanish MICIN under contract PID2021-127890NB-I00 and support from GSI-Darmstadt computing facilities. F. Browne acknowledges a support from the Special Postdoctoral Researcher program of RIKEN. J. Kim acknowledges a support from NRF of the Republic of Korea under Grant No. 2018R1A5A1025563. P. Reiter acknowledges funding from the German BMBF under contracts 05P18PKCIA and 'Verbundprojekt' 05P21PKCII. R. Taniuchi acknowledges funding from The Royal Society. Fruitful discussions with A. Jungclauss are acknowledged.

#### Declaration of competing interest

The authors declare the following financial interests/personal relationships which may be considered as potential competing interests:

Byul Moon reports financial support was provided by National Research Foundation of Korea. Pieter Doornenbal reports equipment, drugs, or supplies was provided by Institute of Modern Physics Chinese Academy of Sciences. Kathrin Wimmer reports financial support was provided by Japan Society for the Promotion of Science. Kathrin Wimmer reports financial support was provided by Spain Ministry of Science and Innovation. Kathrin Wimmer reports financial support was provided by European Research Council. Peter Reiter reports financial support was provided by German Federal Ministry of Education and Research. Ryo Taniuchi reports financial support was provided by The Royal Society. Jiseok Kim reports financial support was provided by National Research Foundation of Korea. Tomas R. Rodríguez reports financial support was provided by Spain Ministry of Science and Innovation. If there are other authors, they declare that they have no known competing financial interests or personal relationships that could have appeared to influence the work reported in this paper.

#### Data availability

Data will be made available on request.

#### References

- [1] M.G. Mayer, *Phys. Rev.* 74 (1948) 235–239.
- [2] M.G. Mayer, *Phys. Rev.* 75 (1949) 1969–1970.
- [3] O. Haxel, J.H.D. Jensen, H.E. Suess, *Phys. Rev.* 75 (1949) 1766.
- [4] F. Nowacki, A. Obertelli, A. Poves, *Prog. Part. Nucl. Phys.* 120 (2021) 103866.
- [5] National Nuclear Data Center, Brookhaven National Laboratory, <http://www.nndc.bnl.gov>.
- [6] P. Federman, S. Pittel, *Phys. Rev. C* 20 (1979) 820–829.
- [7] T. Otsuka, T. Suzuki, R. Fujimoto, H. Grawe, Y. Akaishi, *Phys. Rev. Lett.* 95 (2005) 232502.
- [8] T. Otsuka, *Phys. Scr.* 2013 (T152) (2013) 014007.
- [9] T. Otsuka, Y. Tsunoda, *J. Phys. G, Nucl. Part. Phys.* 43 (2) (2016) 024009.
- [10] J.P. Delaroche, M. Girod, J. Libert, H. Goutte, S. Hilaire, S. Péru, N. Pillet, G.F. Bertsch, *Phys. Rev. C* 81 (2010) 014303.

- [11] N. Paul, A. Corsi, A. Obertelli, P. Doornenbal, G. Authélet, H. Baba, B. Bally, M. Bender, D. Calvet, F. Château, S. Chen, J.-P. Delaroche, A. Delbart, J.-M. Gheller, A. Giganon, A. Gillibert, M. Girod, P.-H. Heenen, V. Lapoux, J. Libert, T. Motobayashi, M. Niikura, T. Otsuka, T.R. Rodríguez, J.-Y. Roussé, H. Sakurai, C. Santamaria, M. Shimizu, D. Steppenbeck, R. Taniuchi, T. Togashi, Y. Tsunoda, T. Uesaka, T. Ando, T. Arici, A. Blazhev, F. Browne, A.M. Bruce, R. Carroll, L.X. Chung, M.L. Cortés, M. Dewald, B. Ding, F. Flavigny, S. Franchoo, M. Górská, A. Gottardo, A. Jungclaus, J. Lee, M. Lettmann, B.D. Linh, J. Liu, Z. Liu, C. Lizarazo, S. Momiyama, K. Moschner, S. Nagamine, N. Nakatsuka, C. Nita, C.R. Nobs, L. Olivier, Z. Patel, Z. Podolyák, M. Rudigier, T. Saito, C. Shand, P.-A. Söderström, I. Stefan, R. Orlandi, V. Vaquero, V. Werner, K. Wimmer, Z. Xu, *Phys. Rev. Lett.* 118 (2017) 032501.
- [12] J. Ha, T. Sumikama, F. Browne, N. Hinohara, A.M. Bruce, S. Choi, I. Nishizuka, S. Nishimura, P. Doornenbal, G. Lorusso, P.-A. Söderström, H. Watanabe, R. Daido, Z. Patel, S. Rice, L. Sinclair, J. Wu, Z.Y. Xu, A. Yagi, H. Baba, N. Chiga, R. Carroll, F. Didierjean, Y. Fang, N. Fukuda, G. Gey, E. Ideguchi, N. Inabe, T. Isobe, D. Kameda, I. Kojouharov, N. Kurz, T. Kubo, S. Lalkovski, Z. Li, R. Lozeva, H. Nishibata, A. Odahara, Z. Podolyák, P.H. Regan, O.J. Roberts, H. Sakurai, H. Schaffner, G.S. Simpson, H. Suzuki, H. Takeda, M. Tanaka, J. Taprogge, V. Werner, O. Wieland, *Phys. Rev. C* 101 (2020) 044311.
- [13] T. Sumikama, K. Yoshinaga, H. Watanabe, S. Nishimura, Y. Miyashita, K. Yamaguchi, K. Sugimoto, J. Chiba, Z. Li, H. Baba, J.S. Berryman, N. Blasi, A. Bracco, F. Camera, P. Doornenbal, S. Go, T. Hashimoto, S. Hayakawa, C. Hinke, E. Ideguchi, T. Isobe, Y. Ito, D.G. Jenkins, Y. Kawada, N. Kobayashi, Y. Kondo, R. Krücken, S. Kubono, G. Lorusso, T. Nakano, M. Kurata-Nishimura, A. Odahara, H.J. Ong, S. Ota, Z. Podolyák, H. Sakurai, H. Scheit, K. Steiger, D. Steppenbeck, S. Takano, A. Takashima, K. Tajiri, T. Teranishi, Y. Wakabayashi, P.M. Walker, O. Wieland, H. Yamaguchi, *Phys. Rev. Lett.* 106 (2011) 202501.
- [14] J. Dobaczewski, I. Hamamoto, W. Nazarewicz, J.A. Sheikh, *Phys. Rev. Lett.* 72 (1994) 981–984.
- [15] K.L. Kratz, B. Pfeiffer, O. Arndt, S. Hennrich, A. Wöhr, t. ISOLDE/IS333, I. Collaborations, the ISOLDE/IS333, *Eur. Phys. J. A* 25 (1) (2005) 633–638.
- [16] T. Togashi, Y. Tsunoda, T. Otsuka, N. Shimizu, *Phys. Rev. Lett.* 117 (2016) 172502.
- [17] P. Doornenbal, P. Reiter, H. Grawe, T. Saito, A. Al-Khatib, A. Banu, T. Beck, F. Becker, P. Bednarczyk, G. Benzoni, A. Bracco, A. Bürger, L. Caceres, F. Camera, S. Chmel, F. Crespi, H. Geissel, J. Gerl, M. Górská, J. Greife, H. Hübel, M. Kavatsyuk, O. Kavatsyuk, M. Kmiecik, I. Kojouharov, N. Kurz, R. Lozeva, A. Maj, S. Mandal, W. Meczynski, B. Million, Z. Podolyák, A. Richard, N. Saito, H. Schaffner, M. Seidlitz, T. Striepling, J. Walker, N. Warr, H. Weick, O. Wieland, M. Winkler, H. Wollersheim, *Nucl. Instrum. Methods Phys. Res., Sec. A* 613 (2) (2010) 218–225.
- [18] T. Kubo, D. Kameda, H. Suzuki, N. Fukuda, H. Takeda, Y. Yanagisawa, M. Ohtake, K. Kusaka, K. Yoshida, N. Inabe, T. Ohnishi, A. Yoshida, K. Tanaka, Y. Mizoi, *Prog. Theor. Exp. Phys.* 2012 (1) (2012) 03C003.
- [19] N. Fukuda, T. Kubo, T. Ohnishi, N. Inabe, H. Takeda, D. Kameda, H. Suzuki, *Nucl. Instrum. Methods Phys. Res., Sec. B* 317 (2013) 323–332.
- [20] K. Wimmer, P. Doornenbal, N. Aoi, H. Baba, F. Browne, C. Campbell, H. Crawford, H.D. Witte, C. Fransen, H. Hess, S. Iwazaki, J. Kim, A. Kohda, T. Koiwai, B. Mauss, B. Moon, T. Parry, P. Reiter, D. Suzuki, R. Taniuchi, S. Thiel, Y. Yamamoto, *RIKEN Accel. Prog. Rep.* 54 (2021) S27.
- [21] N. Warr, J. Van de Walle, M. Albers, F. Ames, B. Bastin, C. Bauer, V. Bildstein, A. Blazhev, S. Bönig, N. Bree, B. Bruyneel, P.A. Butler, J. Cederkäll, E. Clément, T.E. Cocolios, T. Davinson, H. De Witte, P. Delahaye, D.D. DiJulio, J. Diriken, J. Eberth, A. Ekström, J. Elseviens, S. Emhofer, D.V. Fedorov, V.N. Fedosseev, S. Franchoo, C. Fransen, L.P. Gaffney, J. Gerl, G. Georgiev, R. Gernhäuser, T. Grahn, D. Habs, H. Hess, A.M. Hurst, M. Huyse, O. Ivanov, J. Iwanicki, D.G. Jenkins, J. Jolie, N. Kesteloot, O. Kester, U. Köster, M. Krauth, T. Kröll, R. Krücken, M. Lauer, J. Leske, K.P. Lieb, R. Lutter, L. Maier, B.A. Marsh, D. Mücher, M. Münch, O. Niedermaier, J. Pakarinen, M. Pantea, G. Pascovici, N. Patronis, D. Pauwels, A. Petts, N. Pietralla, R. Raabe, E. Rapisarda, P. Reiter, A. Richter, O. Schaile, M. Scheck, H. Scheit, G. Schrieder, D. Schwalm, M. Seidlitz, M. Seliverstov, T. Sieber, H. Simon, K.H. Speidel, C. Stahl, I. Stefanescu, P.G. Thirolf, H.G. Thomas, M. Thürauf, P. Van Duppen, D. Voulot, R. Wadsworth, G. Walter, D. Weißhaar, F. Wenander, A. Wiens, K. Wimmer, B.H. Wolf, P.J. Woods, K. Wrzosek-Lipska, K.O. Zell, *Eur. Phys. J. A* 49 (2013) 40.
- [22] W. Hua, N.T. Zhang, M.L. Liu, Y. Zheng, Y.D. Fang, X.H. Zhou, Y.H. Zhang, X.G. Lei, Y.X. Guo, *Nucl. Struct. China* 2012 (2013) 98–100.
- [23] D. Weisshaar, D. Bazin, P. Bender, C. Campbell, F. Recchia, V. Bader, T. Baugher, J. Belange, M. Carpenter, H. Crawford, M. Cromaz, B. Elman, P. Fallon, A. Forney, A. Gade, J. Harker, N. Kobayashi, C. Langer, T. Lauritsen, I. Lee, A. Lemasson, B. Longfellow, E. Lunderberg, A. Macchiavelli, K. Miki, S. Momiyama, S. Noji, D. Radford, M. Scott, J. Sethi, S. Stroberg, C. Sullivan, R. Titus, A. Wiens, S. Williams, K. Wimmer, S. Zhu, *Nucl. Instrum. Methods Phys. Res., Sec. A* 847 (2017) 187–198.
- [24] S. Paschalis, I. Lee, A. Macchiavelli, C. Campbell, M. Cromaz, S. Gros, J. Pavan, J. Qian, R. Clark, H. Crawford, D. Doering, P. Fallon, C. Lionberger, T. Loew, M. Petri, T. Stezelberger, S. Zimmermann, D. Radford, K. Lagergren, D. Weisshaar, R. Winkler, T. Glasmacher, J. Anderson, C. Beausang, *Nucl. Instrum. Methods Phys. Res., Sec. A* 709 (2013) 44–55.
- [25] S. Agostinelli, J. Allison, K. Amako, J. Apostolakis, H. Araujo, P. Arce, M. Asai, D. Axen, S. Banerjee, G. Barrand, F. Behner, L. Bellagamba, J. Boudreau, L. Broglia, A. Brunengo, H. Burkhardt, S. Chauvie, J. Chuma, R. Chytráček, G. Cooperman, G. Cosmo, P. Degtyarenko, A. Dell'Acqua, G. Depaola, D. Dietrich, R. Enami, A. Felicciolo, C. Ferguson, H. Fesefeldt, G. Folger, F. Foppiano, A. Forti, S. Garelli, S. Giani, R. Giannitrapani, D. Gibin, J. Gómez Cadenas, I. González, G. Gracia Abril, G. Greeniaus, W. Greiner, V. Grichine, A. Grossheim, S. Guatelli, P. Gumplinger, R. Hamatsu, K. Hashimoto, H. Hasui, A. Heikkinen, A. Howard, V. Ivanchenko, A. Johnson, F. Jones, J. Kallenbach, N. Kanaya, M. Kawabata, Y. Kawabata, M. Kawaguti, S. Kelner, P. Kent, A. Kimura, T. Kodama, R. Kokoulin, M. Kossov, H. Kurashige, E. Lamanna, T. Lampén, V. Lara, V. Lefebvre, F. Lei, M. Liendl, W. Lockman, F. Longo, S. Magni, M. Maire, E. Medernach, K. Minamimoto, P. Mora de Freitas, Y. Morita, K. Murakami, M. Nagamatsu, R. Nartallo, P. Nieminen, T. Nishimura, K. Ohtsubo, M. Okamura, S. O'Neale, Y. Oohata, K. Paech, J. Perl, A. Pfeiffer, M. Pia, F. Ranjard, A. Rybin, S. Sadilov, E. Di Salvo, G. Santin, T. Sasaki, N. Savvas, Y. Sawada, S. Scherer, S. Sei, V. Sirotenko, D. Smith, N. Starkov, H. Stoecker, J. Sulkimo, M. Takahata, S. Tanaka, E. Tcherniaev, E. Safai Tehrani, M. Tropeano, P. Truscott, H. Uno, L. Urban, P. Urban, M. Verderi, A. Walkden, W. Wander, H. Weber, J. Wellisch, T. Wenaus, D. Williams, D. Wright, T. Yamada, H. Yoshida, D. Zschesche, *Nucl. Instrum. Methods Phys. Res., Sec. A* 506 (3) (2003) 250–303.
- [26] L. Riley, D. Weisshaar, H. Crawford, M. Agiorgousis, C. Campbell, M. Cromaz, P. Fallon, A. Gade, S. Gregory, E. Haldeman, L. Jarvis, E. Lawson-John, B. Roberts, B. Sadler, C. Stine, *Nucl. Instrum. Methods Phys. Res., Sec. A* 1003 (2021) 165305.
- [27] K. Wimmer, Uchicari, <https://www.nishina.riken.jp/collaboration/SUNFLOWER/devices/hrarray>.
- [28] F. James, Minuit function minimization and error analysis reference manual, <https://root.cern.ch/download/minuit.pdf>.
- [29] D. Kameda, T. Kubo, T. Ohnishi, K. Kusaka, A. Yoshida, K. Yoshida, M. Ohtake, N. Fukuda, H. Takeda, K. Tanaka, N. Inabe, Y. Yanagisawa, Y. Gono, H. Watanabe, H. Otsu, H. Baba, T. Ichihara, Y. Yamaguchi, M. Takechi, S. Nishimura, H. Ueno, A. Yoshimi, H. Sakurai, T. Motobayashi, T. Nakao, Y. Mizoi, M. Matsushita, K. Ieki, N. Kobayashi, K. Tanaka, Y. Kawada, N. Tanaka, S. Deguchi, Y. Satou, Y. Kondo, T. Nakamura, K. Yoshinaga, C. Ishii, H. Yoshii, Y. Miyashita, N. Uematsu, Y. Shiraki, T. Sumikama, J. Chiba, E. Ideguchi, A. Saito, T. Yamaguchi, I. Hachiuma, T. Suzuki, T. Moriguchi, A. Ozawa, T. Ohtsubo, M.A. Famiano, H. Geissel, A.S. Nettleton, O.B. Tarasov, D. Bazin, B.M. Sherrill, S.L. Manikonda, J.A. Nolen, *Phys. Rev. C* 86 (2012) 054319.
- [30] L.M. Robledo, T.R. Rodríguez, R.R. Rodríguez-Guzmán, *J. Phys. G, Nucl. Part. Phys.* 46 (2019) 013001.
- [31] T. Sumikama, A. Bruce, F. Browne, et al., in preparation.
- [32] G. Pasqualato, S. Ansari, J.S. Heines, V. Modamio, A. Görge, W. Korten, J. Ljungvall, E. Clément, J. Dudouet, A. Lemasson, T.R. Rodríguez, J.M. Allmond, T. Arici, K.S. Beckmann, A.M. Bruce, D. Doherty, A. Esmaylzadeh, E.R. Gamba, L. Gerhard, J. Gerl, G. Georgiev, D.P. Ivanova, J. Jolie, Y.H. Kim, L. Knafla, A. Korichi, P. Koseoglou, M. Labiche, S. Lalkovski, T. Lauritsen, H.J. Li, L.G. Pedersen, S. Pietri, D. Ralet, J.M. Regis, M. Rudigier, S. Saha, E. Sahin, S. Siem, P. Singh, P.A. Söderström, C. Theisen, T. Torniy, M. Vandebrouck, W. Witt, M. Zielinska, D. Barrios, P. Bednarczyk, G. Benzoni, A.J. Boston, H.C. Boston, A. Bracco, B. Cederwall, M. Ciemala, G. de France, C. Domingo-Pardo, J. Eberth, A. Gadea, V. González, A. Gottardo, L.J. Harkness-Brennan, H. Hess, D.S. Judson, A. Jungclaus, S.M. Lenzi, S. Leoni, R. Menegazzo, D. Mengoni, C. Michelagnoli, D.R. Napoli, J. Nyberg, Z. Podolyák, A. Pullia, F. Recchia, P. Reiter, K. Rezyznikina, M.D. Salsac, E. Sanchis, M. Şenyiğit, M. Siciliano, J. Simpson, D. Sohler, O. Stezowski, J.J. Valiente-Dobón, D. Verney, *Eur. Phys. J. A* 59 (2023) 276.
- [33] B. Moon, W. Korten, K. Wimmer, et al., in preparation.
- [34] C.M. Baglin, *Nucl. Data Sheets* 113 (8) (2012) 1871–2111.
- [35] J. Chen, B. Singh, *Nucl. Data Sheets* 177 (2021) 1–508.
- [36] H. Xiaolong, *Nucl. Data Sheets* 108 (6) (2007) 1093–1286.
- [37] J. Dechargé, D. Gogny, *Phys. Rev. C* 21 (1980) 1568–1593.
- [38] J. Berger, M. Girod, D. Gogny, *Comput. Phys. Commun.* 63 (1) (1991) 365–374.
- [39] B. Pritychenko, M. Birch, B. Singh, M. Horoi, *At. Data Nucl. Data Tables* 107 (2016) 1–139.
- [40] A. Davydov, G. Filippov, *Nucl. Phys.* 8 (1958) 237.
- [41] N. Shimizu, Y. Tsunoda, Y. Utsuno, T. Otsuka, *Phys. Rev. C* 103 (2021) 014312.
- [42] T. Otsuka, K. Yanase, in a private communication.